Int. J. Electrochem. Sci., 15 **(2020)** 3955 – 3968, doi: 10.20964/2020.05.31

International Journal of
ELECTROCHEMICAL
SCIENCE
www.electrochemsci.org

Effect of Heat Treatment on Thermal Expansion Behavior and Corrosion Resistance of Martensitic Stainless Steel Manufactured by Submerged Arc Welding

Xinyue Wang[1], *Jihui Wang*[1], *Zhiming Gao*[1,*], *Wenbin Hu*[1,2,*]

[1] Tianjin Key Laboratory of composite & Functional Materials, School of Materials Science and Engineering, Tianjin University, Tianjin, 300072, China
[2] Key Laboratory of Advanced ceramics and Machining Technology (Ministry of Education), Tianjin University, Tianjin, 300072, China
[*]E-mail: gaozhiming@tju.edu.cn; wbhu@tju.edu.cn

Received: 3 February 2020 / *Accepted:* 11 March 2020 / *Published:* 10 April 2020

The martensitic stainless steel surfacing layer was deposited on the H13 steel using submerged arc welding (SAW). The effect of the tempering conditions (350 ℃ ~ 650 ℃ for 2 h and 450 ℃ for 0.5 h ~ 4 h) on the microstructure, thermal expansion behavior and corrosion resistance was systematically analyzed. The results indicated that tempering led to the transformation of the residual austenite and coarse martensite in the as-welded sample to the fine tempered martensite and carbides (Fe_3C-450 ℃/0.5 h and M_7C_3-other conditions). An optimal fusion between the H13 steel and surfacing layer was obtained in all cases, with no appreciable cracks. Relative thermal expansion ($\Delta L/L_0$) and thermal expansion coefficient (CTE) were observed to increase at first due to the reduction in the welding defects, followed by a decrease due to the phase transition and microstructure coarsening on increasing the tempering temperature and duration. The thermal expansion behavior closest to that of the H13 steel was obtained at 450 ℃ for 2 h, along with a better thermal stability and lower cracking sensitivity. Furthermore, the surfacing layer with a high alloy content exhibited much better corrosion resistance than the H13 steel. After tempering at or above 450 ℃ for 2 h, the corrosion resistance of the surfacing layers was noted to be higher than the as-welded sample. The corrosion resistance enhanced further on increasing the tempering temperature and duration, which was dependent on the even phase composition and homogeneous microstructure as well as decreased welding defects and grain boundaries. The maximum R_{ct} value (1.961×10^5 $\Omega\cdot cm^2$) was obtained at 650 ℃ for 2 h, thus, suggesting an optimal corrosion resistance.

Keywords: H13 steel, submerged arc welding, martensitic stainless steel, tempering, thermal expansion, corrosion resistance.

1. INTRODUCTION

H13 steel with high strength, ductility, wear resistance and impact toughness has been widely used in the manufacturing of dies [1-3]. These dies are subjected to complex loads during service, which result in a heavy damage on the surface, such as excessive wear, cracks and corrosion [4-6]. Some extreme consequences can result if such damages are not addressed effectively.

Martensitic stainless steels are commonly used for repairing and manufacturing the dies by surfacing technology owing to advantages of low cost, high deposition rate and surface appearance [7,8]. The generated surfacing layer has specific properties required by the industrial production processes, such as high hardness as well as wear and corrosion resistance [9,10]. However, the chemical composition of the surfacing layer is different from that of the substrate, which causes significant thermal and microstructural stresses during surfacing, post-welding heat treatment or application, thereby, resulting in cracking and peeling of the surfacing layer [11]. The thermal expansion coefficient (CTE) is a key index to evaluate the cracking sensitivity of the materials [12]. Low CTE value indicates good dimensional stability and low cracking sensitivity of the materials. However, in case the CTE of the surfacing layer is much lower than that of the substrate, the excessive compressive stress leads to the cracking of the substrate. Therefore, the surfacing layer with CTE close to the substrate is recommended.

In addition, some welding defects and residual stresses in the welding area have an adverse impact on the performance, which necessitates the use of the post-welding tempering process [11,13]. A few research studies [14-16] have indicated that the microstructure and properties of the welding area are sensitive to the tempering temperature and duration. Increasing the tempering temperature and duration has been observed to reduce the microhardness and enhance the impact toughness of the welds with martensite structure [17-18]. However, Shiue et al. [15] reported that the microhardness of the welds exhibited an increase as a result of the secondary hardening caused by the carbide precipitation during tempering. Besides, the moderate tempering temperature and duration can improve the thermal expansion behavior and corrosion resistance of the martensitic stainless steels [19-23]. Previous works [8,24] have demonstrated that the surfacing layer of the martensitic stainless steel was deposited on the H13 steel using submerged arc welding (SAW), and its mechanical properties were improved by adjusting the tempering temperature. The results indicated an enhanced refinement of the microstructure for the sample tempered at 450 ℃, demonstrating high comprehensive mechanical properties. However, the mechanisms involving the impact of the post-weld tempering process on the thermal expansion behavior and corrosion resistance of the surfacing layer have not been explained clearly. In this study, the surfacing layers were tempered at 350 ℃ ~ 650 ℃ for 2 h and 450 ℃ for 0.5 h ~ 4 h, respectively, and the microstructural characteristics, thermal expansion behavior and corrosion resistance were investigated.

2. EXPERIMENTAL

2.1 Materials and processes

Surfacing trials were performed on H13 steel with chemical composition of 0.32C-0.87Si-0.32Mn-5.32Cr-1.32Mo-0.88V-0.016P-0.001S-bal.Fe (units in mass%). Acetone was applied to remove

grease from H13 steel and derust by pickling. A flux-cored wire of 3.2 mm in diameter that consists of ferrochrome, ferromolybdenum and ferrovanadium, was used for SAW, and other process parameters refer to previous work [8]. The surfacing layer generated was tempered at 350 ℃, 450 ℃, 550℃, 650 ℃ for 2 h and 450 ℃ for 0.5 h, 1 h, 2 h, 4 h followed by air-cooling. The chemical composition of the surfacing layer is shown in Table 1.

Table 1. Chemical composition of the surfacing layer (wt.%).

C	Si	Mn	Cr	Mo	V	Ni	Fe
0.06	0.51	1.17	13.10	0.48	0.08	1.50	balance

2.2 Characterization

The microstructural characteristics of the surfacing layer were observed using a transmission electron microscopy (TEM, Tecnai, F30) and scanning electron microscope (SEM, SU1510) with energy dispersive spectrometer (EDS). The phase composition was detected by an X-ray diffractometer (XRD, Brook, D8) using Cu Ka radiation from 20° to 90°.

Thermal expansion tests by following GB/T 4339-2008 standard were performed using a dilatometer from 32 ℃ to 800 ℃ with heating rate of 5 ℃/min in an argon atmosphere. The dimensions of the sample is Φ7 mm × 25 mm.

Electrochemical measurements were conducted by a VersaSTAT3 electrochemical system in 3.5 wt.% NaCl solution at room temperature with a traditional three electrode system. The working electrode is H13 steel substrate and the surfacing layers subjected to different tempering processes, with an exposed area being 1 cm^2. The counter electrode and reference electrode were the platinum plate and saturated calomel electrode (SCE), respectively. The potentiodynamic polarization curves and electrochemical impedance spectra (EIS) were employed to evaluate the corrosion resistance of the surfacing layers. The sweep rate of the polarization curve is 0.5 mV/s. The frequency range of EIS measurement is 100 kHz ~ 10 mHz, and the amplitude is 10 mV. Before testing, the surfacing layers were immersed in the electrolyte for 5 h for a stable open circuit potential and passive film.

3. RESULTS AND DISCUSSION

3.1 Microstructure

A previous study [24] has investigated the microstructural evolution of the surfacing layer of the martensitic stainless steel tempered at 350 ℃ ~ 650 ℃ for 2 h and indicated that the as-welded microstructure of the surfacing layer was composed of the coarse martensite, lower bainite, residual austenite and second phase particles ($M_{23}C_6$ phase). On increasing the tempering temperature, the number of the welding defects decreased, and the plate-like martensite and residual austenite transformed into fine needle-like tempered martensite and new second phase particles (M_7C_3 phase). Similarly, the phase structures of the surfacing layers tempered at 450 ℃ for 0.5 h ~ 4 h are shown in Fig. 1. The α-Fe phase was detected in the surfacing layer before and after tempering, which presented

three well-defined peaks at 44.8°, 65.1° and 82.3° corresponding to the crystallographic planes (110), (200) and (211), respectively. The γ-Fe phase occurring in the as-welded sample was not detected in the tempered samples, owing to the decomposition of the residual austenite during tempering [14]. In addition, the Fe_3C phase was found only in the sample tempered for 0.5 h. Guo [25] reported that the alloying elements in the alloy steel were redistributed as the tempering temperature exceeded 400 ℃, and the martensite dissolution was accompanied by the Fe_3C phase precipitation. On increasing the tempering duration, a part of the Fe_3C phase was dissolved into the matrix again, while the remaining Fe_3C was converted to other carbides.

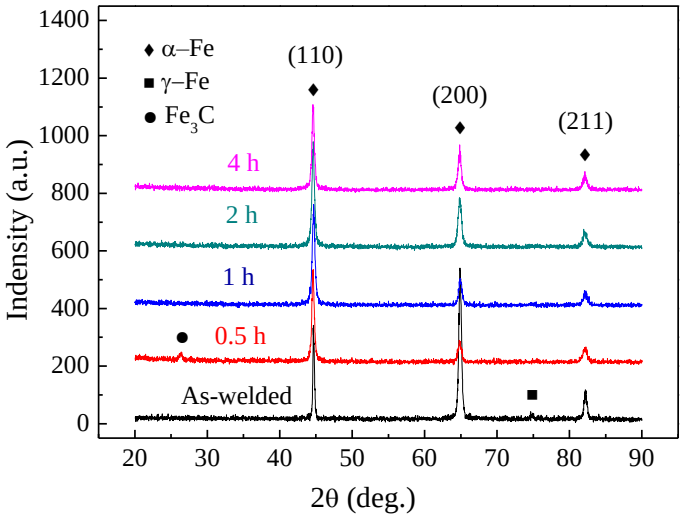

Figure 1. XRD spectra of the surfacing layers tempered at 450 ℃ for different tempering durations.

Fig. 2 presents the TEM micrographs showing the microstructure of the surfacing layers in the as-welded condition for different tempering durations. It is obvious that tempering changed the microstructural characteristics of the surfacing layer to a large extent. In case the surfacing layer was tempered for 0.5 h, the number of dislocations in the martensite laths decreased, and the residual austenite transformation and decomposition of the martensite laths occurred. As a result, fragmented tempered martensite was observed (SAED in Fig. 2(h)), and a large number of the second phase particles were observed to be uniformly dispersed in the matrix (Fig. 2(d)). From Fig. 1, these second phase particles were identified as the Fe_3C phase. However, along with a large fraction of the Fe_3C phase, a small M_7C_3 phase was also detected in the sample tempered for 1 h (Fig.s 2(e) and (i)), which is consistent with the findings reported by Guo [25]. The fraction of the tempered martensite and M_7C_3 phase distributed on the laths and grain boundaries increased with the tempering duration, whereas the proportions of the residual austenite and dislocations decreased [26], resulting in a fine and homogeneous microstructure for the tempering duration reaching 2 h, as shown in Fig.s 2(e-g). However, a coarsening of the microstructure was observed due to the grain growth (Fig.2(g)) with further increase in the tempering duration. The EDS analysis indicates that the $M_{23}C_6$ and M_7C_3 phases consisted of different contents of C, Cr, Fe, Mo, V, Ni and W elements (Fig. 3), which is consistent with the previous study [24].

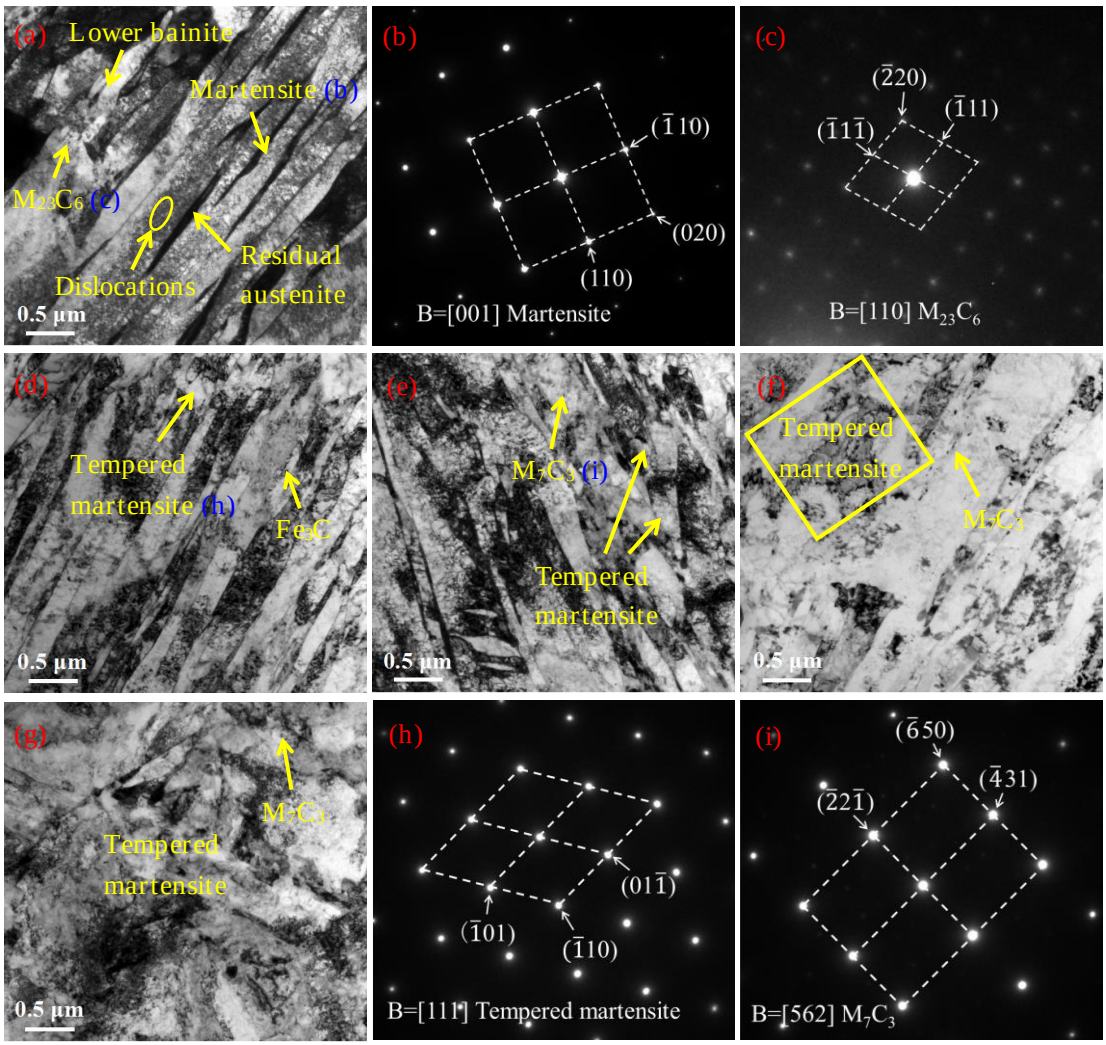

Figure 2. TEM micrographs showing the microstructure of the surfacing layers: the as-welded sample (a) and tempering samples at 450℃ for 0.5 h (d), 1 h (e), 2 h (f), 4 h (g); SAED of martensite (b), M23C6 (c) , tempered martensite (h) and M7C3 (i).

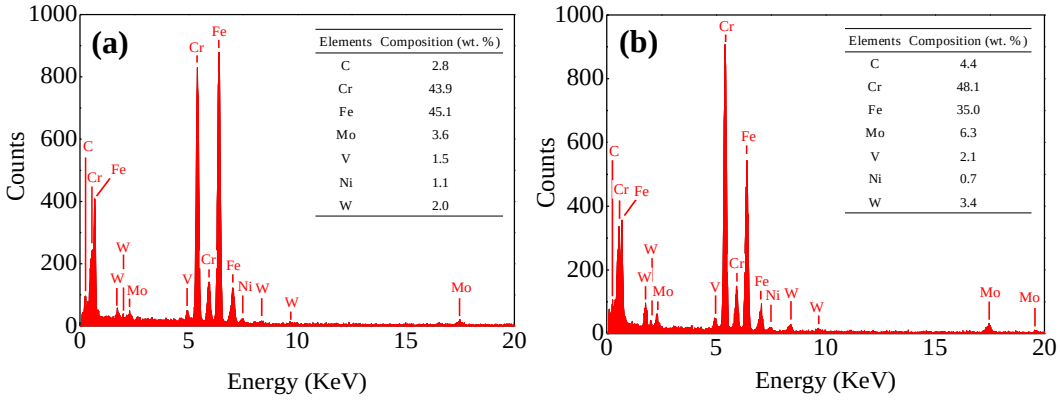

Figure 3. EDS analysis of $M_{23}C_6$ (a) and M_7C_3 (b).

Fig. 4 shows the cross-sectional morphology of the interface positions between the H13 steel and surfacing layers for different tempering processes. As observed in Fig. 4(a), the H13 steel and surfacing

layer combined tightly after surfacing, which was characterized by the uneven microstructure and clear boundary resulting due to the relatively rapid cooling rate, however, no appreciable cracks were observed. Tempering led to the microstructural changes and diffusion of its alloy elements [24]. The corresponding boundary became blurred on increasing the tempering temperature and duration, withc complete disappearance for the specimen tempered at 450 ℃ for 2 h, as shown in Fig. 4(b). Nevertheless, Fig. 4(c) and (d) show that an excessive tempering led to the reappearance of the boundary, which might be attributed to the unsynchronized grain growth processes. Overall, an optimal fusion between the H13 steel and surfacing layer was obtained in all cases.

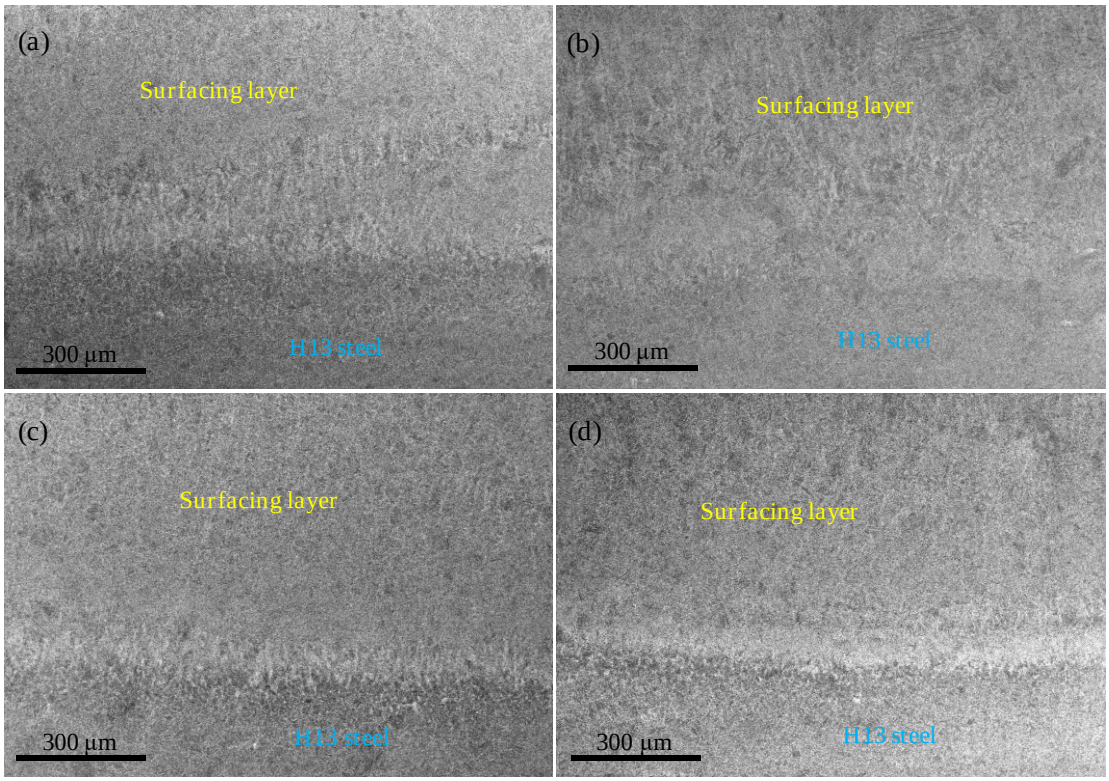

Figure 4. Cross-sectional morphologies of interface positions between H13 steel and surfacing layer in the as-welded condition (a) and after tempering at 450 ℃ for 2 h (b) or 4 h (c), 650 ℃ for 2 h (d).

3.2 Thermal expansion behavior

Fig. 5 shows the relative thermal expansions ($\Delta L/L_0$) and thermal expansion coefficients (CTE) of H13 steel and surfacing layers under different tempering conditions. As seen, the surfacing layer shows a better thermal stability and lower cracking sensitivity than that of H13 steel, which was characterized by a lower $\Delta L/L_0$ and CTE values resulting in a compressive stress [12]. After tempering, $\Delta L/L_0$ and CTE values of the surfacing layers increased slightly, showing a tendency closed to that of H13 steel, which may be attributable to the changes of microstructure and welding defects in the surfacing layer. In detail, tempering reduces the residual compressive stress and dislocation density of the surfacing layer, resulting in the increase of the thermal expansion during reheating because it is able to withstand higher thermal stress before cracking. The maximum CTE value of the surfacing layer with

a fine and homogeneous microstructure was obtained at 450 ℃ for 2 h. Further increasing the tempering temperature and duration, the CTE value decreased due to microstructure coarsening caused by grain growth. Besides, the residual austenite transformation and martensite decomposition into tempered martensite accompanied with carbides precipitation can cause the decrease of CTE value [19,27,28]. That is, thermal expansion behaviors of the surfacing layers tempered at 350 ℃ ~ 450 ℃ for 2 h or 450 ℃ for 0.5 h ~ 2 h were mainly affected by the residual stress and dislocation density in the surfacing layer, indicating an increase in thermal expansion, whereas the thermal expansion decreased with further increasing the tempering temperature and duration due to the phase transition and microstructure coarsening [28].

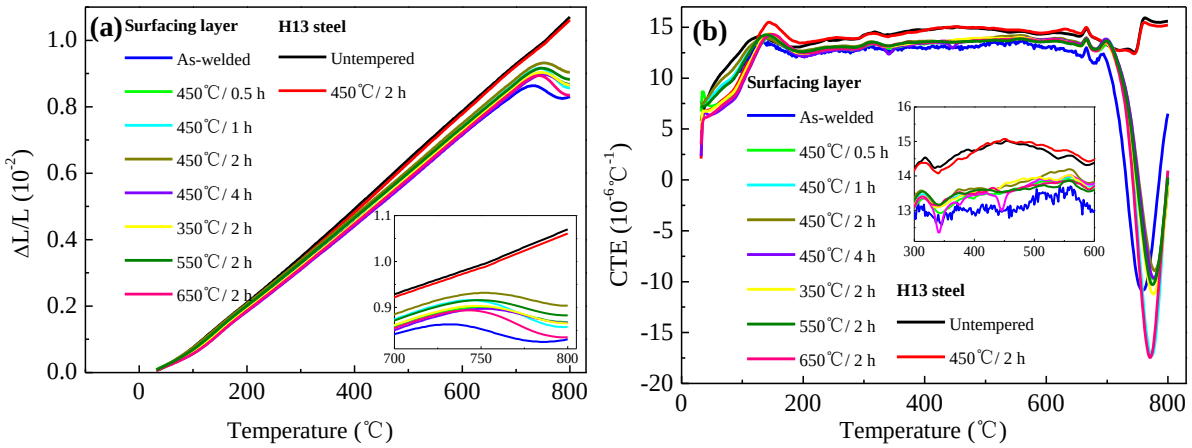

Figure 5. $\Delta L/L_0$ (a) and CTE (b) values of H13 steel and surfacing layers under different tempering conditions.

Furthermore, CTE values of H13 steel and surfacing layers change greatly due to the experimental error in the initial stage of 32 ℃ ~ 200 ℃. The $\Delta L/L_0$ value of H13 steel increased linearly from 200 ℃ to 800 ℃, and CTE value fluctuates around a stable constant, showing no phase transition occurred. The thermal expansion of H13 steel was mainly caused by thermal effect from 32 ℃ ~ 800 ℃. As for surfacing layer, the similar tendency involved to the thermal expansion was observed before the inflection point of 730 ℃. But the $\Delta L/L_0$ and CTE values fluctuate strongly when the temperature rises above 730 ℃, which was analyzed using XRD at high temperature, indicating a transformation of α-Fe phase into γ-Fe phase, as shown in Fig. 6. The slope of relative thermal expansion decreased due to the austenitization from 730 ℃ to 750 ℃. The increasing value indicates that the thermal effect causing thermal expansion dominates. Further increasing the reheating temperature, the volume contraction caused by austenitization plays a dominant role. As a result, the thermal expansion of the surfacing layer decreased until the end of austenitization. In addition, the increasing difference in the thermal expansion between H13 steel and surfacing layer may cause cracking in H13 steel when the temperature exceeds 750 ℃.

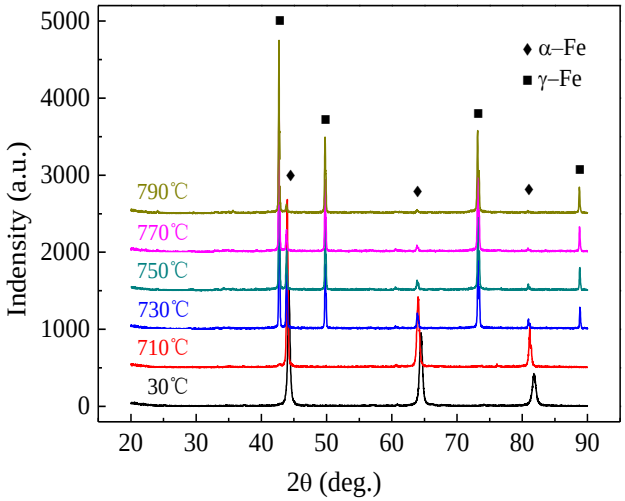

Figure 6. High temperature XRD spectra of the surfacing layer tempered at 450 ℃ for 2 h.

3.3 Corrosion Resistance

Fig. 7 shows the potentiodynamic polarization curves of the H13 steel and surfacing layers under different tempering conditions, with the corresponding electrochemical parameters shown in Table 2. The surfacing layer deposited on the H13 steel exhibited a higher corrosion potential (E_{coor}) and lower corrosion current density (j_{corr}), suggesting an excellent corrosion resistance. Besides, the passive regions were observed on the anode polarization curves of the surfacing layers. The formation of the passive films containing chromium further enhanced the corrosion resistance of the sample. As observed, the tempering changed the corrosion resistance of the surfacing layers in varying degrees, which was characterized by the different electrochemical corrosion parameters (Table 2). The E_{coor}, j_{corr} and pitting potential (E_p) of the as-welded surfacing layer were noted to be -0.179 V, 0.399 μA·cm^{-2} and 0.021 V, respectively. As the tempering temperature increased from 350 ℃ to 650 ℃ for 2 h, the E_{coor} of the surfacing layers increased from -0.175 V to -0.085 V, with the j_{corr} decreasing from 0.277 μA·cm^{-2} to 0.129 μA·cm^{-2}, thus, exhibiting an increase in the corrosion resistance [29]. Besides, the increasing E_p value suggested that the protective effect of the passive film on the matrix was enhanced gradually. However, the corrosion resistance of the surfacing layers tempered at 450 ℃ for 0.5 h and 1 h was inferior to the as-welded sample. The corresponding E_{coor} were -0.300 V and -0.272 V, and the j_{corr} were 1.730 μA·cm^{-2} and 1.043 ± 0.07 μA·cm^{-2}. On increasing the tempering duration, the corrosion resistance was observed to improve. After tempering at or above 450 ℃ for 2 h, the corrosion resistance of the tempered surfacing layer was noted to be higher than that of the as-welded sample. In summary, on enhancing the tempering temperature and duration, j_{corr} was observed to decrease, while E_{coor} and E_p increased gradually, thus, indicating enhanced corrosion resistance of the surfacing layers.

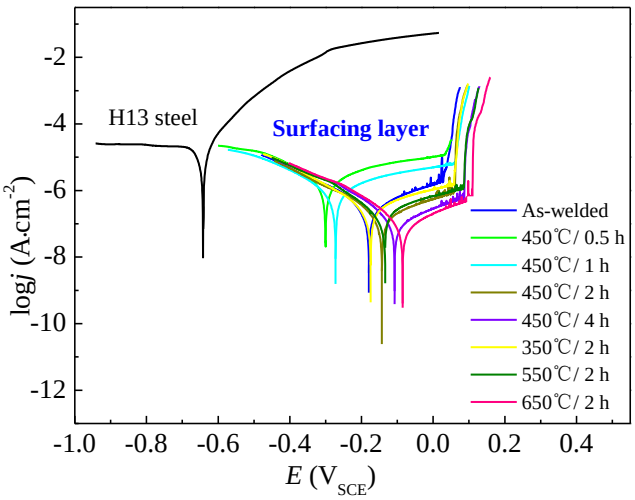

Figure 7. Potentiodynamic polarization curves of H13 steel and surfacing layers under different tempering conditions.

Table 2. Electrochemical parameters obtained from Figure 7.

Samples		j_{corr} (μA·cm^{-2})	E_{coor}/V$_{SEC}$	E_p/V$_{SEC}$
H13 steel		53.37	-0.642	-
Surfacing layer	As-welded	0.399	-0.179	0.021
	450 ℃/0.5 h	1.730	-0.300	0.034
	450 ℃/1 h	1.043	-0.272	0.062
	450 ℃/2 h	0.257	-0.143	0.065
	450 ℃/4 h	0.165	-0.108	0.091
	350 ℃/2 h	0.277	-0.175	0.065
	550 ℃/2 h	0.184	-0.134	0.093
	650 ℃/2 h	0.129	-0.085	0.115

It is well understand that chloride ions in corrosive media tend to be adsorbed on dislocations and grain boundaries, and corrosion occurs preferentially at these defects [30]. Moreover, the residual stress in the surfacing layer can accelerate the corrosion process [20,31]. So more welding defects existed in the as-welded sample, such as dislocations and residual stress, led to a poor corrosion resistance. When the surfacing layers were tempered at 450 ℃ for 0.5 h and 1 h, the insufficient tempering results in a slight reduction in the welding defects with the residual austenite decomposition. Man et al. [20] reported that the residual austenite distributed along the martensite lath boundaries can prevent the propagation of intergranular corrosion, thereby increase the corrosion resistance of martensitic stainless steel. On the contrary, the reduction of residual austenite content weakened the corrosion resistance of the surfacing layer. Moreover, the transformation of coarse martensite into fine tempered martensite led to the increase of grain boundaries during tempering, thereby decreased the corrosion resistance of the surfacing layer. Further increasing the tempering temperature and duration, the corrosion resistance of the surfacing layer was increased, which can be mainly attributed to the reduction of the welding defects and grain boundaries caused by grain growth. It is worth noting that carbides contents increased with the tempering temperature and duration (Fig. 2). Some researchers believed carbides precipitation

containing chromium element led to the Cr-depletion regions, where are sensitive to corrosion attack due to uneven passive films formation [20,32,33]. However, the result in this study shows the increase of the protective effect of passive film based on the increasing E_p values, which can be attributed to the low carbon content in the surfacing layer (Table 1) causing a slight effect on the corrosion resistance of the surfacing layer. Above all, the corrosion resistance of the surfacing layer in this study mainly depends on phase composition, the number of welding defects and grain boundaries, as well as compact and homogeneous microstructure.

Fig. 8 shows the surface morphology and cross-sectional element distribution of the surfacing sample tempered at 650 ℃ for 2 h after the polarization curve. The surfacing sample was taken out as the current density reach to 1 mA ·cm^{-2}. From Fig. 8(a), a few pits were observed on the corroded surface due to the passive film breakdown when the potential reaches the pitting potential. However, the pit size is different, which may be due to the different breakdown times of passive films. Man et al. [20] reported that the uneven passive films formed in the Cr-depletion regions was first broken down, and then other regions follow. Furthermore, the cross-sectional element distribution at one of the pits of the surfacing sample was analyzed, as shown in Fig. 8(b), reporting that the contents of chromium, nickel and manganese elements of the surfacing layer are significantly higher than that of H13 steel, on the contrary, the other elements are lower, which is consistent with the result of Table 1. The elements present an uneven distribution at the interface of H13 steel and surfacing layer after tempering due to incomplete diffusion. Moreover, the contents of alloy elements in pitting region is slightly smaller than that in non-pitting region of the surfacing layer [32].

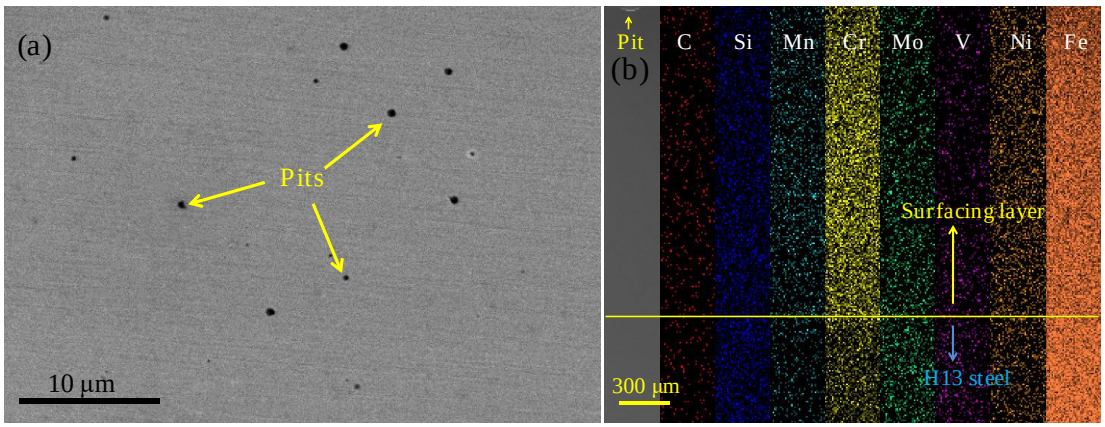

Figure 8. Surface morphology (a) and cross-sectional element distribution (b) of the surfacing sample tempered at 650 ℃ for 2 h after the polarization curve.

The EIS measurements were conducted at room temperature in 3.5 wt.% NaCl solution, and the results present in the Nyquist and Bode plots, as shown in Fig. 9. From Fig. 9(a), the semicircles of all samples were displayed in the first quadrant, suggesting the characteristics of capacitive impedance arc. And the radius of the impedance arc of the surfacing layer is much larger than for H13 steel. As known, the larger the radius of the impedance arc, the better the corrosion resistance of the sample. So the surfacing layer has a better corrosion resistance than H13 steel. When the tempering temperature increased from 350 ℃ to 650 ℃ for 2 h, the radius of the impedance arc was increased gradually,

indicating an increasing corrosion resistance. But when the surfacing layers were tempered at 450 ℃ for 0.5 h and 1 h, showing a poor corrosion resistance than the as-welded sample based on a smaller radius of the impedance arc. Increasing the tempering duration, the radius is larger than that of the as-welded sample, showing an increase in corrosion resistance. The conclusion is consistent with the results of the potentiodynamic polarization curves.

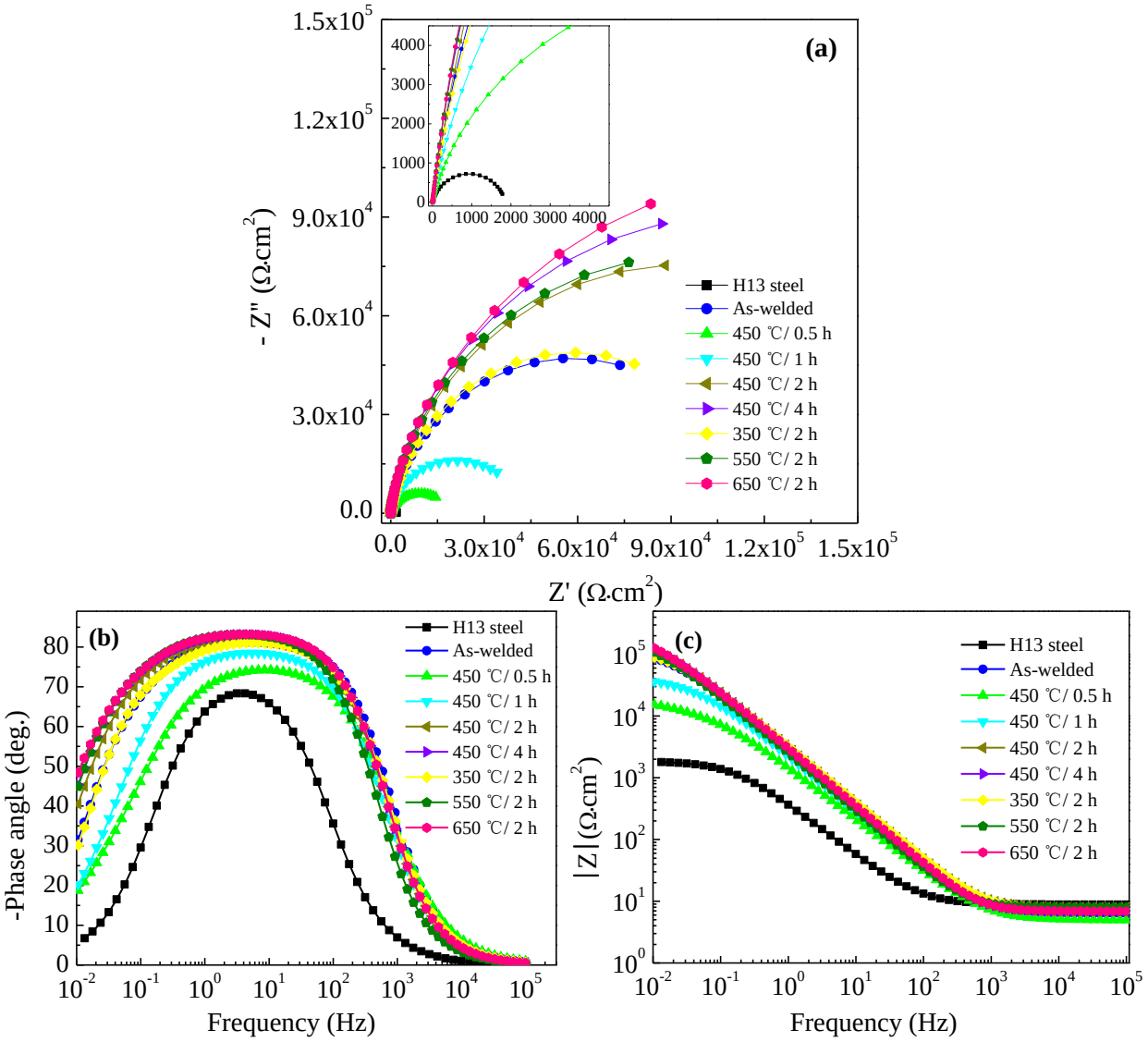

Figure 9. Nyquist (a), Bode-phase (b) and Bode-|Z| (c) plots of H13 steel and surfacing layers with different tempering processes.

As seen from Fig. 9(b) and (c), Bode plots show one time constant for H13 steel corresponding to the dissolution of the substrate, but two time constants were observed in the surfacing layer, which indicate the corrosion behavior of the surfacing layer go through two chemical reaction processes in 3.5 wt.% NaCl solution. The first one at high frequencies reveals the passivity breakdown and repassivating processes of passive films. The second one appearing at low frequencies is related to the dissolution of the surfacing layer. Fig. 10(a) is the quivalent circuit for H13 steel to simulate the measured impedance

data, and Fig. 10(b) is the quivalent circuit for the surfacing layers. In which R_s is the electrolyte resistance between the working electrode and reference electrode, Q_{dl} is constant phase angle element representing double layer capacitance for H13 steel in Fig. 10(a) or the surfacing layers in Fig. 10(b), R_{ct} represents the charge transfer resistance. R_c and Q_c are the resistance and capacitance of the passive film at high frequency. $n_1$and n_2 are the effect parameter of Q_c and $Q_{dl,}$ whose ideal conditions are 1 as to a completely parallel capacitor. The higher R_{ct} and R_c values mean better corrosion resistance. The detailed fitting parameters and corresponding errors are shown in Table 3. As seen from Table 3, the similar values of the R_s (4.954 $\Omega \cdot cm^2$ ~ 8.822 $\Omega \cdot cm^2$) between H13 steel and surfacing layers were obtain in 3.5 wt.% NaCl solution, with the little difference being caused by the deviation of the solution and the reference electrode [34]. The corrosion resistance of the surfacing layer is higher than that of H13 steel, which was characterized by a higher R_{ct} value. Besides, the R_{ct} value of the surfacing layer increased gradually with the increase of the tempering temperature and duration, with the maximum value (1.961×10^5 $\Omega \cdot cm^2$) being obtained at 650 ℃ for 2 h, suggesting the best corrosion resistance [35]. It is likely to due to the reduction of the welding defects and grain boundaries caused by grain growth after tempering at a high temperature. Furthermore, when the tempering temperature exceeds 450 ℃ for 2 h, the R_c values are higher than that of the as-welded sample and maintain a high value with further increasing the temperature and duration, indicating an increase in the protective effect of passive films [36].

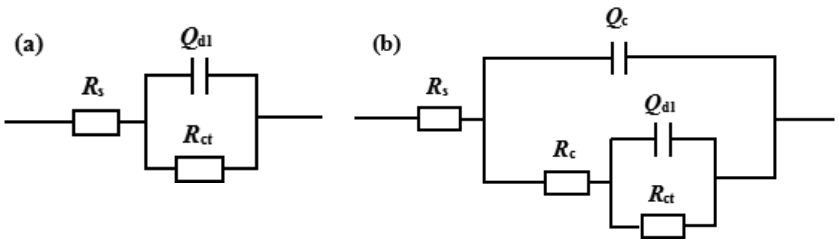

Figure 10. Equivalent circuits for H13 steel (a) and surfacing layers (b).

Table 3 EIS fitting parameters of H13 steel and surfacing layers.

Samples		R_s ($\Omega \cdot cm^2$)	Q_c ($10^{-5}F \cdot cm^{-2}$)	n_1	R_c ($10^4\Omega \cdot cm^2$)	Q_{dl} ($10^{-5}F \cdot cm^{-2}$)	n_2	R_{ct} ($10^3\Omega \cdot cm^2$)
H13		8.822	-	-	-	54.83	0.8432	1.853
Surfacing layer	As-welded	6.304	6.046	0.9232	5.507	4.062	0.7639	60.44
	450℃/0.5h	4.954	1.401	0.8500	1.148	44.61	0.6275	8.383
	450 ℃/1 h	7.191	8.566	0.8904	3.390	44.77	0.6853	11.34
	450 ℃/2 h	7.872	5.895	0.9156	10.36	3.749	0.7300	82.13
	450 ℃/4 h	6.937	5.919	0.9358	6.591	1.852	0.6828	159.5
	350 ℃/2 h	7.579	5.747	0.9162	5.029	2.471	0.8007	66.02
	550 ℃/2 h	7.873	6.942	0.9368	7.464	2.782	0.7173	115.0
	650 ℃/2 h	6.868	5.928	0.9354	8.255	2.280	0.6302	196.1

4. CONCLUSIONS

(1) The surfacing layer in the as-welded condition consisted of the coarse martensite, lower bainite, residual austenite and $M_{23}C_6$ (M=Cr, Fe, Mo, V, Ni and W), with a mass of dislocations distributing on the martensite laths. Tempering (350℃ ~ 650℃ for 2 h and 450℃ for 0.5 ~ 4 h) led to the transformation from the residual austenite and coarse martensite to the fine tempered martensite and carbides, with a decrease in the welding defects. The Fe_3C phase was detected in the surfacing layer tempered at 450 ℃ for 0.5 h, whereas the M_7C_3 phase was observed in other tempering processes. Thus, a fine and homogeneous microstructure was obtained at 450 ℃ for 2 h. Further increasing the tempering temperature and duration caused microstructure coarsening, however, an optimal fusion between the H13 steel and surfacing layer was obtained, with no appreciable cracks observed in any case.

(2) The surfacing layer with low $\Delta L/L_0$ and CTE values exhibited better thermal stability and lower cracking sensitivity than the H13 steel. The CTE closest to that of the H13 steel material was obtained at 450 ℃ for 2 h owing to a fine and homogeneous microstructure with a low crack tendency. Moreover, the differences in the $\Delta L/L_0$ and CTE values between the H13 steel and surfacing layer increased as the reheating temperature exceeded 750 ℃ due to austenitization.

(3) The surfacing layer exhibited much better corrosion resistance than that of the H13 steel. A passive region was observed on the anode polarization curve of the surfacing layer. The surfacing layers tempered at 450 ℃ for 0.5 h and 1 h demonstrated inferior corrosion resistance than the as-welded sample due to the insufficient tempering. Further enhancing the tempering temperature and duration improved the corrosion resistance of the surfacing layers due to the reduction of the welding defects and grain boundaries, with the maximum R_{ct} value (1.961×10^5 $\Omega\cdot cm^2$) obtained at 650 ℃ for 2 h, thus, suggesting an optimal corrosion resistance.

ACKNOWLEDGEMENTS
This work was supported by National Natural Science Foundation of China (51671144, 51871164); Shandong Taishan Industry Leading Talents Project (SF1503302301); Supporting Plan Project of Tianjin City (16YFZCGX00100); Science and Technology Plan Project of Tianjin City (18YFZCGX00050).

References

1. M.X. Wei, S.Q. Wang, L. Wang, X.H. Cui, K.M. Chen, *Tribol. Int.*, 44 (2011) 898.
2. A.G. Ning, W.W. Mao, X.C. Chen, H.J. Guo, J. Guo, *Metals*, 7 (2017) 70.
3. J. Sjöström, J. Bergström, *J. Mater. Process. Technol.*, 153 (2004) 1089.
4. J.H. Peng, Z.Z. Zhu, D.Y. Su, *Tribol. Int.*, 129 (2019) 232.
5. B. Wang, X.F. Zhao, W.Z. Li, M. Qin, J.F. Gu, *Appl. Surf. Sci.*, 431 (2018) 39.
6. T.F. Rütti, G. Piskoty, R. Koller, L. Wullschleger, S.A. Michel, *Eng. Fail. Anal.*, 14 (2007) 1103.
7. K. Yang, Z.X. Zhang, W.Q. Hu, Y.F. Bao, Y.F. Jiang, *J. Iron Steel Res. Int.*, 18 (2011) 74.
8. X.Y. Wang, J.H. Wang, Z.M. Gao, D.H. Xia, W.B. Hu, *J. Mater. Process. Technol.*, 262 (2018) 182.
9. J.Y. Park, Y.S. Park, *Corrosion*, 62 (2006) 541.
10. C.K. Lin, W.C. Fan,W.J. Tsai, *Corrosion*, 58 (2002) 904.
11. V. Lazić, D. Arsić, R.R. Nikolić, B. Hadzima, *Procedia Eng.*, 153 (2016) 392.

12. H.J. Xie, X.C. Wu, Y.A. Min, *J. Iron Steel Res. Int.*, 15 (2008) 56.
13. C.M. Lin C, C.Z. Huang, C.Y. Su, C.S. Chen, *Mater. Lett.*, 204 (2017) 89.
14. J. Yang, Y.L. Yang, Y.F. Zhou, X.W. Qi, X.J. Ren, Q.X. Yang, *Surf. Coat. Technol.*, 219 (2013) 69.
15. R.K. Shiue, K.C. Lan, C. Chen, *Mater. Sci. Eng. A*, 287 (2000) 10.
16. C.M. Lin, C.H. Lu, *Mater. Sci. Eng. A*, 676 (2016) 28.
17. B. Huang, J.Y. Zhang, Q.S. Wu, *J. Nucl. Mater.*, 490 (2017) 115.
18. J.Y. Zhang, B. Huang, Q.S. Wu, C.J. Li, Q.Y. Huang, *Fusion Eng. Des.*, 100 (2015) 334.
19. T. Waterschoot, K. Verbeken, B.C. De Cooman, *ISIJ Int.*, 46 (2006) 138.
20. C. Man , C.F. Dong, D.C. Kong, L. Wang, X.G. Li, *Corros. Sci.*, 151 (2019) 108.
21. S.D. Ban, Y.T. Shin, S.R. Lee, H.W. Lee, *Int. J. Electrochem. Sci.*, 11 (2016) 7764.
22. Y.R. Liu, D. Ye, Q.L. Yong, J. Su, K.Y. Zhao, W. Jiang, *J. Iron Steel Res. Int.*, 18 (2011) 60.
23. B. Sunil Kumar, V. Kain, B. Vishwanadh, *Corrosion*, 73 (2016) 362.
24. X.Y. Wang, J.H. Wang, Z.M. Gao, D.H. Xia, W.B. Hu, *J. Mater. Process. Technol.*, 269 (2019) 26.
25. K.X. Guo, *Acta Metall. Sin.*, 2 (1957) 303. (in Chinese)
26. D.C. Saha, E. Biro, A.P. Gerlich, Y. Zhou, *Mater. Sci. Eng. A*, 673 (2016) 467.
27. S.M.C. Van Bohemen, J. Sietsma, *Mater. Sci. Tech-Lond.*, 30 (2014) 1024.
28. S.M.C. Van Bohemen, *Scripta Mater.*, 75 (2014) 22.
29. L.Y. Xu, M. Li, H.Y. Jing, Y.D. Han, *Int. J. Electrochem. Sci.*, 8 (2013) 2069.
30. I. Taji, M.H. Moayed, M. Mirjalili, *Corros. Sci.*, 92 (2015) 301.
31. X.W. Lei, Y.R. Feng, J.X. Zhang, A.Q. Fu, C.X. Yin, D.D. Macdonald, *Electrochim. Acta*, 191 (2016) 640.
32. S.X. Li, Y.N. He, S.R. Yu, P.Y. Zhang, *Corros. Sci.*, 66 (2013) 211.
33. C.C. Pan, Y. Song, W.X Jin, Z.B. Qin, S.Z. Song, W.B Hu, D.H. Xia, *Trans.Tianjin Univ.*, https://doi.org/10.1007/s12209-020-00238-8.
34. D.T. Cai, S.G. Han, S.D. Zheng, Z.Y. Luo, Y.P. Zhang, K. Wang, *J. Mater. Process. Technol.*, 255 (2018) 530.
35. J. Song, Z.M. Gao, C.X. Liu, Z.H. Liu, W.B. Hu, *Int. J. Electrochem. Sci.*, 15 (2020) 879.
36. A.S. Hamdy, E. El-Shenawy, T. El-Bitar, *Int. J. Electrochem. Sci.*, 1 (2006) 171.